ResearchOnline@JCU

JAMES COOK UNIVERSITY
AUSTRALIA

Forced turbulent fountain flow behavior

N. WILLIAMSON[1], S.W. ARMFIELD[1], AND WENXIAN LIN[2]

[1]School of Aerospace, Mechanical and Mechatronic Engineering, The University of Sydney, NSW, 2006 AUSTRALIA

[2]School of Engineering & Physical Sciences, James Cook University, Townsville, Queensland, 4811 AUSTRALIA

Numerical simulations of fully turbulent fountain flow are used to investigate the important energy and mass transfer mechanisms present in the forced fountain flow regime, which exists at Froude numbers (Fr) greater than 3. The flow is equivalent to a negatively buoyant jet with three flow streams, the inner upflow (IF), the outer downflow (OF) and the surrounding ambient fluid (AF). The dense fountain fluid rises upward from the source exchanging mass and momentum with OF. The fluid decelerates under gravity and stagnates in the cap region and is forced radially outward into the OF. The OF fluid falls back to the source as a dense plume, entraining fluid from the IF and AF. Once it reaches the lower bounding wall the fluid forms a dense intrusion which grows radially outward.

Simulation results are presented for $Fr = 4$ and 7 at Reynolds number $Re = 3494$. The mean fountain penetration height scales with the previously reported relation $Z_m/R_0 = 2.46Fr$, where R_0 is the source radius. The flow is shown to be much more comlpex than previous studies have suggested with several behaviors observed through the fountain height.

At $Fr = 4$ the annular shear layer around the IF does not merge before the cap region and the flow is not fully developed. At $Fr = 7$ the shear layer merges at $Z/R_0 \approx 10$. In this initial developing region, the IF expands rapidly and entrains ambient fluid and dense fluid from the OF so that the flux of buoyancy increases over $Z/R_0 = 0 - 3$ and mass flux increases over $Z/R_0 = 0 - 4$. From $Z/R_0 = 5 - 12$ the IF expands weakly with weak detrainment into the OF. Above $Z/R_0 = 12$, the IF bulk velocity decreases rapidly with radial flow into the OF. In this region the Reynolds stresses increase relative to the bulk velocity and helical instabilities observed in non-buoyant jets are strongly present in the IF. The radial pressure gradient increases as fluid is forced radially into the OF.

The OF is similar to a pure line plume sourrounding the IF however is more unsteady with irregular xpulsions of fluid from the IF. Over the region $Z/R_0 = 5 - 12$ the length scale for a pure plume appear apply and partial self-similarity exists. The entrainmetn from the AF is $\alpha = 0.1 - 0.2$ approximately in the range for pure plume entrainment.

The result smay be used to develop better models of the flow behavior, particualrly the behavior in the cap region which is poorly understood presently.

Key Words: Fountains, buoynacy driven flow, scaling, entrainment

1. Introduction

In turbulent fountains or jets where a buoyancy force opposes the initial fluid motion, the flow rises to its maximum height and stagnates before forming an outer downflow (OF) which interacts with the inner flow (IF) and the ambient fluid (AF) as illustrated by the schamatic in figure 1. The flow occurs widely in industrial and geophysical flows but is also an example of more general shear mixing flow where buoyancy force is aligned with the flow. Specific attention has been given to flow occurances in air–conditioning and heating in large buildings (Baines *et al.* 1990; Lin & Linden 2005), volcanic eruptions (Kaminski *et al.* 2005; Suzuki *et al.* 2005) and the dynamics of cumulus cloud tops (Turner 1966). Fully turbulent flow is characterised only by the Froude number,

$$Fr = \left(\frac{M_0 W_0}{R_0 F_0} \right)^{1/2}, \tag{1.1}$$

where R_0 is the radius of the source. M_0 and F_0 are the source momentum flux and buoyancy flux defined as

$$M_0 = \int_0^{R_0} 2\pi r(\overline{W}^2)\, dr, \quad F_0 = \int_0^{R_0} 2\pi \sigma r \overline{W}\, dr,$$

where $\overline{W_0}$ is the local time averaged vertical velocity, σ is the reduced gravity between the fountain source and the ambient fluid and is defined as $\sigma = g(\rho_0 - \rho_\infty)/\rho_\infty$, with the subscript 0 indicating a quantity at the fountain source and ∞ a property of the ambient fluid. The characteristic velocity is $W_0 = Q_0/A_0$ with Q_0 and A_0 being the volume flow rate and source cross-sectional area respectively.

Kaye & Hunt (2006) found that the fountain behavior can be classified into three distinct regimes, 'very weak flow' for $Fr \lesssim 1$, 'weak flow' $1 \lesssim Fr \lesssim 3$ and forced flow for $Fr \gtrsim 3$. The identification of these regimes and the corresponding scaling relations for the fountain steady-state penetration depth Z_m, have been the subject of a number of studies (Turner 1966; Mizushina *et al.* 1982; Campbell & Turner 1989; Baines *et al.* 1990; Cresswell & Szczepura 1993; Zhang & Baddour 1997, 1998; Bloomfield & Kerr 2000; Lin & Armfield 2000*a*,*b*; Kaye & Hunt 2006; Williamson *et al.* 2008*a*,*b*; Baddour & Zhang 2009).

For turbulent very weak fountains, the momentum flux is relatively weak so the fountain rises to provide the pressure head to accelerate the flow radially giving $Z_m = f(Q_0, F_0) = C_1 Q_0 F_0^{-1/3}$ or $Z_m/R = C_1 Fr^{2/3}$ (Zhang & Baddour 1997, 1998; Lin & Armfield 2000*b*; Kaye & Hunt 2006; Williamson *et al.* 2010). Williamson *et al.* (2010) showed that for $Fr \gtrsim 0.4$ the contribution of the source velocity head becomes significant. The contribution of the velocity head to the penetration height has the following scaling $Z_m \sim U_0^2/\sigma \equiv M_0^2/Q_0 F_0$ or $Z_m/R \sim Fr^2$ (Zhang & Baddour 1997; Kaye & Hunt 2006; Williamson *et al.* 2010). In this way from $0.4 \lesssim Fr \lesssim 3$ the flow has two behaviors driving the flow so $Z_m/R = C_1 Fr^{2/3} + C_2 Fr^2$. From $Fr \gtrsim 3$ the flow approaches a linear scaling $Z_m/R = C_3 Fr$ or $Z_m \sim M_0^{3/4}/F_0^{1/2}$ first identified by Turner (1966) using dimensional arguments and laboratory experiments. Further experiments by Baines *et al.* (1990) and Mizushina *et al.* (1982) show this relation holds above $Fr \approx 300$. Numerous other experiments support the scaling but there is some variation in the constant coefficient $C_3 = 2.1 - 3.06$ (Turner 1966; Campbell & Turner 1989; Baines *et al.* 1990; Cresswell & Szczepura 1993; Kaye & Hunt 2006; Williamson *et al.* 2008*b*; Baddour & Zhang 2009).

Early experimental studies provide some details of the structure of the flow in the high Fourde number regime. Mizushina *et al.* (1982) used anemometer probes to measure
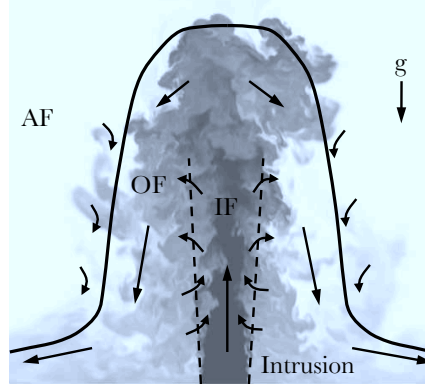
Figure 1: Schematic of fountain flow structure.

point velocity and temperature for fountain flow with $Fr \approx 5 - 260$ and Cresswell & Szczepura (1993) used laser Doppler anemometry and fast themocoulpes to measure turbulent quantities in a $Fr = 3.16$ flow of negatively buoyant hot water jet. Other studies include Sendan *et al.* (1978) who provide temperature measurments only and Demetriou (1978). Mizushina *et al.* (1982) showed that unlike plumes or non-buoyant jets, in fountain flow, both the upflow and downflow continue to develop along their trajectories so the flow never attains self-similarity and the flow statistics vary with axial location and Froude number.

An analytical argument for the linear high Froude number scaling was provided by Kaye & Hunt (2006), who obtained this result using an integral model and assuming entrainment in high Froude number forced fountains is similar to that in non-buoyant jets. Other modelling attempts include the work of Abraham (1967); Bloomfield & Kerr (1998, 2000); Lin & Linden (2005). Bloomfield & Kerr (2000) extended the integral model of Morton (1959) to fountain flow by modifing the entrainment mechanism to include radial entrainment velocity ω from the IF to the OF (ω_β), the OF to the IF (ω_α) and the AF to the OF (ω_γ). The authors suggested two formulations for these entrainment processes. The most sucessful of these was the assumption that ω_α depends on the IF vertical velocity, ω_β on the OF vertical velocity and ω_γ also on the OF vertical velocity only. The corresponding entrainment coeficients for these flow streams, α, β, γ were taken to be constant with height and Froude number. In testing the model they took $\alpha = 0.085$, based on earlier experiments of the initial rise of turbulent fountain flow in Bloomfield & Kerr (1998). The coefficients γ and β were taken to be 0.147, a typical of value for entrainment in a pure line plume. Results obtained by numerical integration of the equations compared well with quantites which are available in Mizushina *et al.* (1982), including the fountain width, velocity in both streams and upflow buoyancy. The model was sensitive to the value of γ.

The apparent success of Bloomfield & Kerr (2000) approach suggests that the behavior of the OF and the IF are essentially de-coupled and can be treated two separate well understood flows, a plume and a jet. Kaye & Hunt (2006) work also supports this idea in that they only consider the upflow, in the limit of a very high Froude number flow, which they take to be behaves like a turbulent jet. The proof of this concept in their work is the obtaining of the established linear Foude number scaling using this model. The understanding of the mixing behavior and the dynamics of the two streams is critical for successful development of scaling models in more complex ambient environments.

Measurements required to understand this behavior are not currently available in the literature. The objective of this work is to give direct evidence for flow behavior in the weak to forced flow regimes particularly over the transition from weak flow to forced flow, for which there is currently litle data available, and give details of the mass and momentum exchanges between the IF, OF and AF. To this end direct numerical simulations of fully turbulent foutnain flow over the range $Fr = 4 - 7$. Our numerical model is described in §2. In §3 the general flow behavior is described and in §4 the rise time and penetration height scaling results are presented. In §5 an alaysis of the entrainment behavior and the momentum transfers is presented. The conclusions are summarised in §7.

2. Numerical formulation

We use direct numerical simulation (DNS) to solve the Navier–Stokes equations for incompressible flow and employ the Boussinesq approximation. The non-dimensionalised continuity, momentum and scalar transport equations are

$$\frac{\partial u_i}{\partial x_i} = 0, \tag{2.1}$$

$$\frac{\partial u_i}{\partial t} + \frac{\partial (u_i u_j)}{\partial x_j} = -\frac{\partial p}{\partial x_i} + \frac{1}{Re}\frac{\partial^2 u_i}{\partial x_j \partial x_j} - \frac{\phi}{Fr_0^2}, \tag{2.2}$$

$$\frac{\partial \phi}{\partial t} + \frac{\partial (u_j \phi)}{\partial x_j} = \frac{1}{RePr}\frac{\partial^2 \phi}{\partial x_j \partial x_j}, \tag{2.3}$$

where Pr is the Prandtl number, the Reynolds number is defined as $Re = U_0 R_0/\nu$ and ν is the kinematic viscosity of the fluid. The velocity (U_i), temperature (θ), pressure (P), time (T) and length (X_i) are made non-dimensional as $u_i = U_i/W_0$, $\phi = (\theta - \theta_\infty)/(\theta_0 - \theta_\infty)$, $p = P/\rho W_0^2$, $t = TW_0/R_0$ and $x_i = X_i/R_0$ respectively.

The discretised governing equations were solved in finite volume form on a non-staggered cartesian grid. The spatial derivatives were discretised using second order central finite differences except for the scalar advective term which is nominally a second order centred scheme but with the ULTRA-flux limiter applied Leonard & Mokhtari (1990). The advective terms were advanced in time using the second order Adams–Bashforth scheme while the viscous terms were advanced using the Crank–Nicolson scheme. Rheichow interpolation was used for the cell face velocities in the pressure solver. The system of equations was solved with the BICGSTAB solver with a Muilti-grid Jacobi preconditioner. The computational domain is a rectangular box in which the top and side walls are open boundaries. The open boundries are open modelled enforcing a zero gradient condition on the velocity and scalar field and zero second derivative on the presure correction term. The bottom boundary is also no-slip/adiabatic, except for the fountain source located in the centre where the normal velocity and temperature have uniform profiles at W_0 and ϕ_0.

We present results for high Froude number flow $Fr = 4$ and 7.0 and $Re = U_0 R_0/\nu = 3350$ with $Pr = 7$ in order to compare with Mizushina *et al.* (1982) and Cresswell & Szczepura (1993) hot water jet studies. The details of the simulations are given in table 1. We also refer to a previous $Fr = 2.1$ simulation presented in Williamson *et al.* (2008*a*, 2010).

A regular cartesian grid is used which is uniform in the horizontal x, y plane within a distance $Lu_{x,y}$ of the centre of the source. Outside this region the grid is streched at approximately 5% growth-rate. The grid is uniform in the axial direction up to Lu_z and

Fr	Pr	Re	$\frac{\Delta X,Y}{R_0}, \frac{\Delta Z}{R_0} \times 10^3$	$\frac{L_{x,y}}{R_0}, \frac{L_z}{R_0}$	$N_{x,y}, N_z$	$\frac{Lu_{x,y}}{R_0}, \frac{Lu_z}{R_0}$
4.0	7.0	3350	30,60	16,17	293,197	3,9.5
7.0	7.0	3350	31,60	20,32	325,325	3.5,17

Table 1: Simulation parameters $\Delta X, Y, Z$, $L_{x,y,z}$ and $N_{x,y,z}$ give the grid size at the source, the domain size and the number of nodes respectively.

streched at 3% thereafter. For the $Fr = 4.0$ and $Fr = 7.0$ simulations, the source is described as a uniform steady inlet profile, while the $Fr = 2.1$ simulation is an unsteady turbulent inlet velocity profile obtained by performing a seperate periodic pipe flow simulation. The details of this work are given in Williamson *et al.* (2010). The ratio of grid cell size ($\Delta X, Y, Z$) to Kolmogorov scale (η) ranges from 1-3.5. The smallest scalar turbulent length scale, $\eta_\phi = \frac{\eta}{\sqrt{\text{Pr}}}$ so DNS spatial resolution requirements are not met here with a Prandtl number of 7. The application of the flux limiter to the advective term provides sufficient damping and prevents non-physical negative temperatures occuring in the present simulations and was not found to be problematic to the solution in Williamson *et al.* (2010).

3. Results

The flow development of the $Fr = 4.0, 7.0$ simulations is shown in Figure 2–3 with contours of ϕ. In both cases the initial transient flow features are interesting. The initial startup flow consists of the rising col024mated IF stream with a the vortex ring rising with the front of the IF. When the fountain reaches its initial maximum height, the ring rises off the top and sheds dense fluid in both $Fr = 4.0$ and 7.0 . At $Fr = 4.0$ the vortex ring detaches from the upflowing fountain but is overcome by bouyancy forces and decends to back to the source. At $Fr = 7.0$ the weaker buoyancy forces allow the structure to rise futher and escape the computational domain. At $Fr = 2.1$ the ring does not detach from the initial upflow. On reaching the maximum initial height the flow reverses and the downflow is established followed by the intrusion along the bounding lower wall. The behavior of the vortex head has been examined for weak fountain flow by Marugán-Cruz *et al.* (2009), with $Fr \approx 0.3 - 1.9$, where the head does not detach. After reaching its maximum initial height the OF forms and the overall fountain height decreases. The fountain then fluctuates about its mean height with none of the instability observed in laminar flow Williamson *et al.* (2008*b*). This behaviour is illustrated in movies 1–2 (available with the online version of the paper).

The structure of the fully developed flow is illustrated in figure 4 (a-b) for $Fr = 2.1$ and 4.0 and in figure 5 for $Fr = 7.0$ with velocity vectors, pressure contours and shading indicating scalar concentrantion. In all the simulations there is a high pressure region where the intrusion forms and the OF meets the bounding wall. For $Fr = 2.1$ and 4.0 the IF is relatively unmixed with ambient fluid. At $Fr = 7.0$ for $z < 10$, the IF is a potential core with mixing in a shear layer between the IF and OF through vortex structures which move through the interface in both up and down the fountain. The low pressure regions and circulation indicated by vectors indicate where vortex structures exist in the instantaneous flow in figure 5. The interaction of the upflow and downflow generate high and low pressure regions forcing the flow to bend in a sinuous way, similar to the helical instability observed in turbulent jets. This occurs both in the potential core and in the
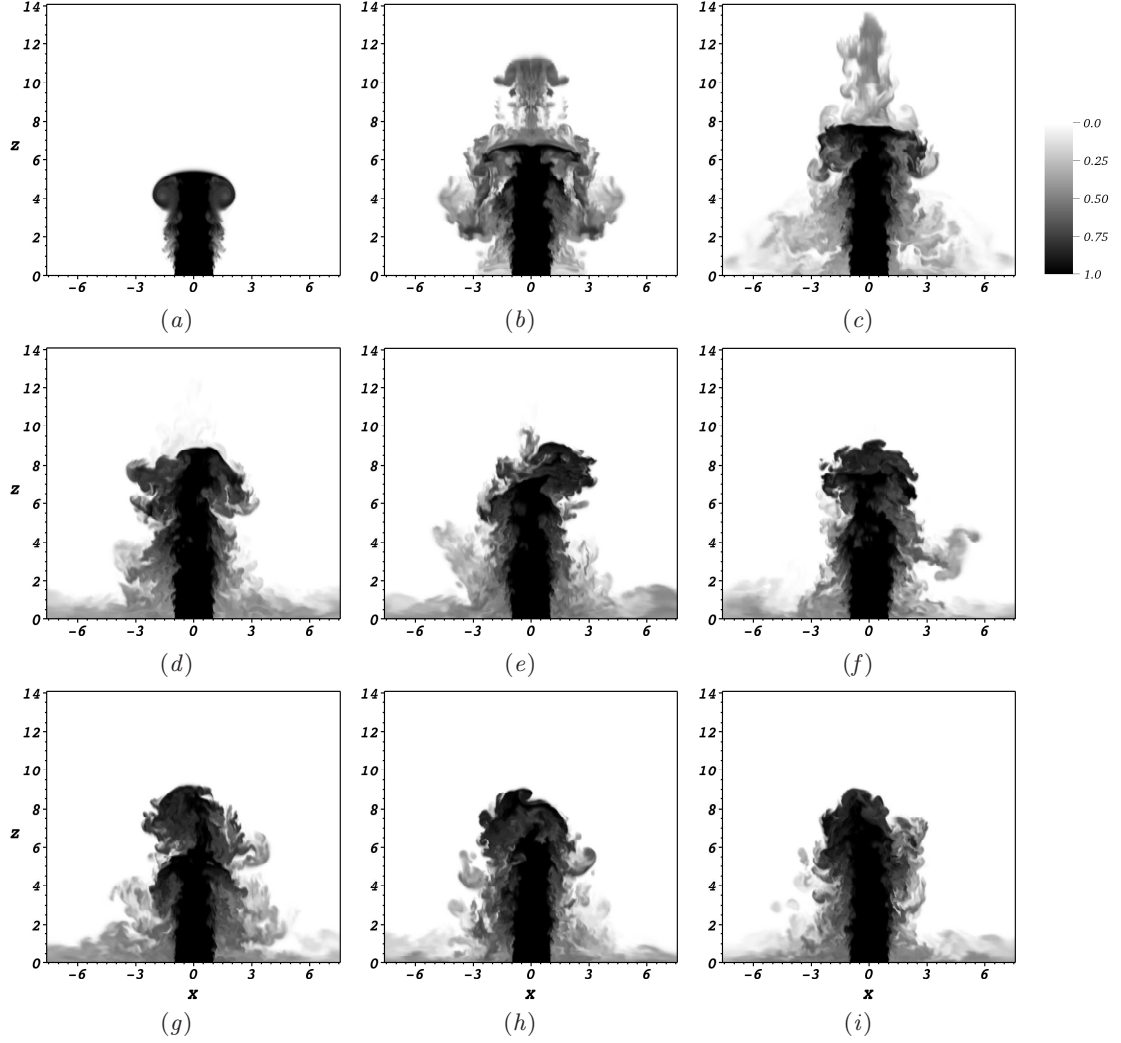
Figure 2: Flow development of $Fr = 4.0$ simulation from $tU_0/R = 12.0$ (a) in increments of $\Delta tU_o/R = 24.5$. Shading indicates ϕ with the scale given above.

head of the fountain. At $z/R = 10$ this sinuous flapping behavior is very strong with the upflow velocity localy weak.

At the head of the fountain the flow is highly unsteady where a vortex ring forms around a rising pulse in the IF and is then shed into the downflow. The ejection and re-entrainment of fluid here is complex. The behavior is approximately periodic with the period of oscialiton of $tU_0/R \approx 37$. The expulsion of fluid from the cap region in antisymmetric pulses down one side or non-uniform annular ejections out around a continually reforming and collapsing vortex ring is a common feature to the $Fr = 2.1, 4.0, 7.0$ simulations. At $Fr = 2.1$ and $Fr = 4$ the IF and cap region is more stable.
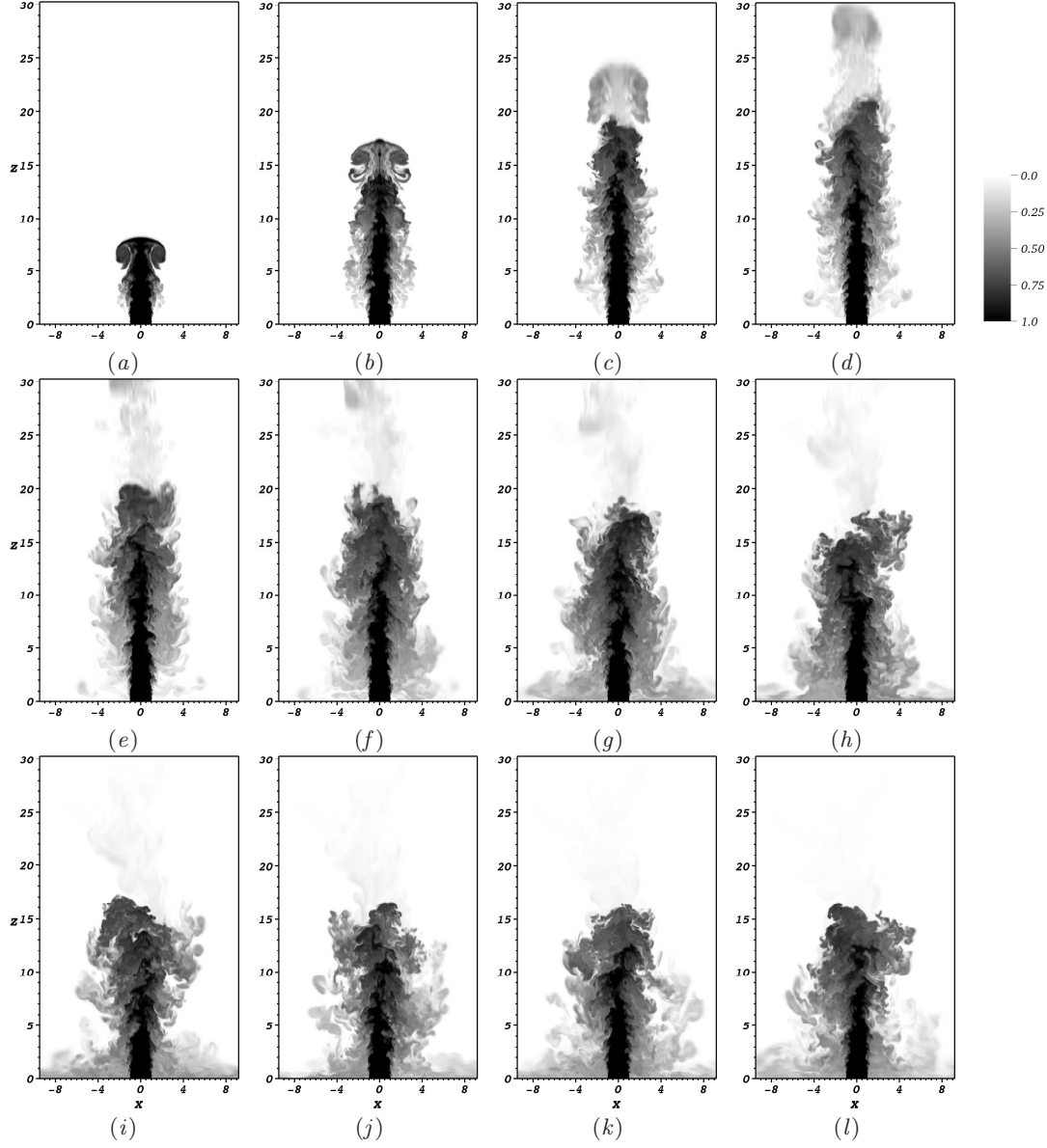
Figure 3: Flow development of $Fr = 7.0$ simulation from $tU_o/R = 16.7$ (a) in increments of $\Delta tU_o/R = 24.5$. Shading indicates ϕ with the scale given above.

4. Initial transient flow behavior

The centerline height of the fountain rises, falls and then rises to its maximum and oscillates about a lower mean value after which flow statistics are obtained. The time trace of the source pressure and the maximum penetration height are given in figure 6. The source pressure is given as this is important quanity for low Froude number flow Williamson *et al.* (2010). The rise time of high Froude number turbulent fountains was shown to scale on $t_m U_0/R \sim Fr^2$ empirically by Pantzlaff and Lueptow Pantzlaff & Lueptow (1999) and then by Williamson *et al.* (2008b) for laminar high Froude number
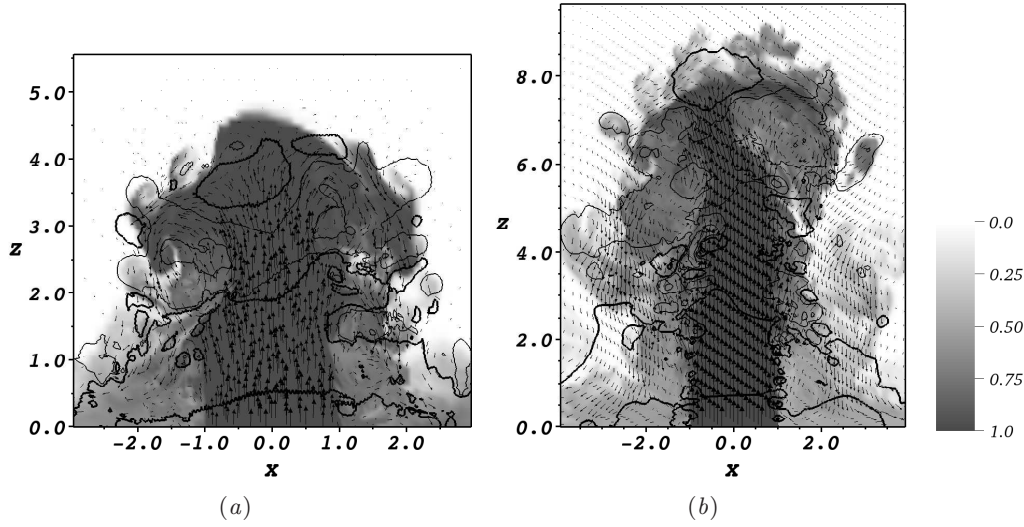
Figure 4: Flow structure of $Fr = 2.1$ flow at $tU_0/R = 36$ (a) and $Fr = 4.0$ flow at $tU_0/R = 174$ (b). Shading indicates ϕ with scale given above and vectors are scaled to give relative velocity magnitude. Thicklines indicate $p/\rho U_0^2$ contors of, 0.03 and 0.25 in (a); 0.1 and 0.02 in (b). Thin lines give $p/\rho U_0^2$ contors of, -0.25 and -0.03 in (a); -0.1 and -0.02 in (b).

fountain flow. This scaling does not collapse the two curves here, possibly becasue the flow regime is close to the transition point, so the time axis is unscaled.

The source pressure is initially negative as the annular vortex at the head of the foutnain rises past the tracer point. The pressure then rises slightly and is nearly constant until the downflow meets the bounding wall and the intrusion forms. At $Fr = 4$ the pressure rises over $tU/R = 25 - 80$ before reaching a constant mean value. The fountain height rises and at $tU/R \approx 35$ the vortex ring detaches and continues to rise and then fall meeting the fountain top at $tU/R \approx 85$. The maximum location along $r = 0$ where $\phi = 0.1$ gives the approximate location of the top of the detached vortex while the minimum location of $\phi = 0.1$ gives approximately the top of the fountain cap region. The fountain reaches steady state behavior at approximately $tU/R \approx 120$ and statisitcs computed over $tU/R \approx 120 - 210$. For $Fr = 7$, the vortex ring seperates at $tU/R \approx 65$, shown in Figure 3 (a). The vortex leaves the top of the domain with some of the fluid returning to the source, meeting the fountain at $tU/R \approx 200$. Flow statistics have been taken over $tU/R \approx 200 - 285$. The source pressure is steady until $tU/R \approx 80$ when it rises as the intrusion forms $tU/R \approx 80 - 150$ and is steady there after.

In figure 7, the fountain mean pentration height, defined as the point where $W = 0$, is plotted against Froude number together with the other published results for this range of Froude numbers. There is a high degree of correspondence between the high Reynolds number simulations in this study and the previous results. From $Fr = 2.1 - 7$ the height moves towards the $z_m = 2.46Fr$ line. The point where the flow can be considered fully forced in not clear from the figure. Zhang & Baddour (1998) performed experiments with round saline/fresh water fountains over the range $850 < Re < 12750$ and $0.37 < Fr < 36.2$ and found for $Fr > 7$ the mean maximum penetration height follows $z_{\max} = 3.06Fr$ but for $Fr < 7$ is better represented by $z_{\max} = 1.7Fr^{1.3}$. Creswell and Szczepura Cresswell & Szczepura (1993) demonstrated that at $Fr = 3.16$ the upflow is dominated by the
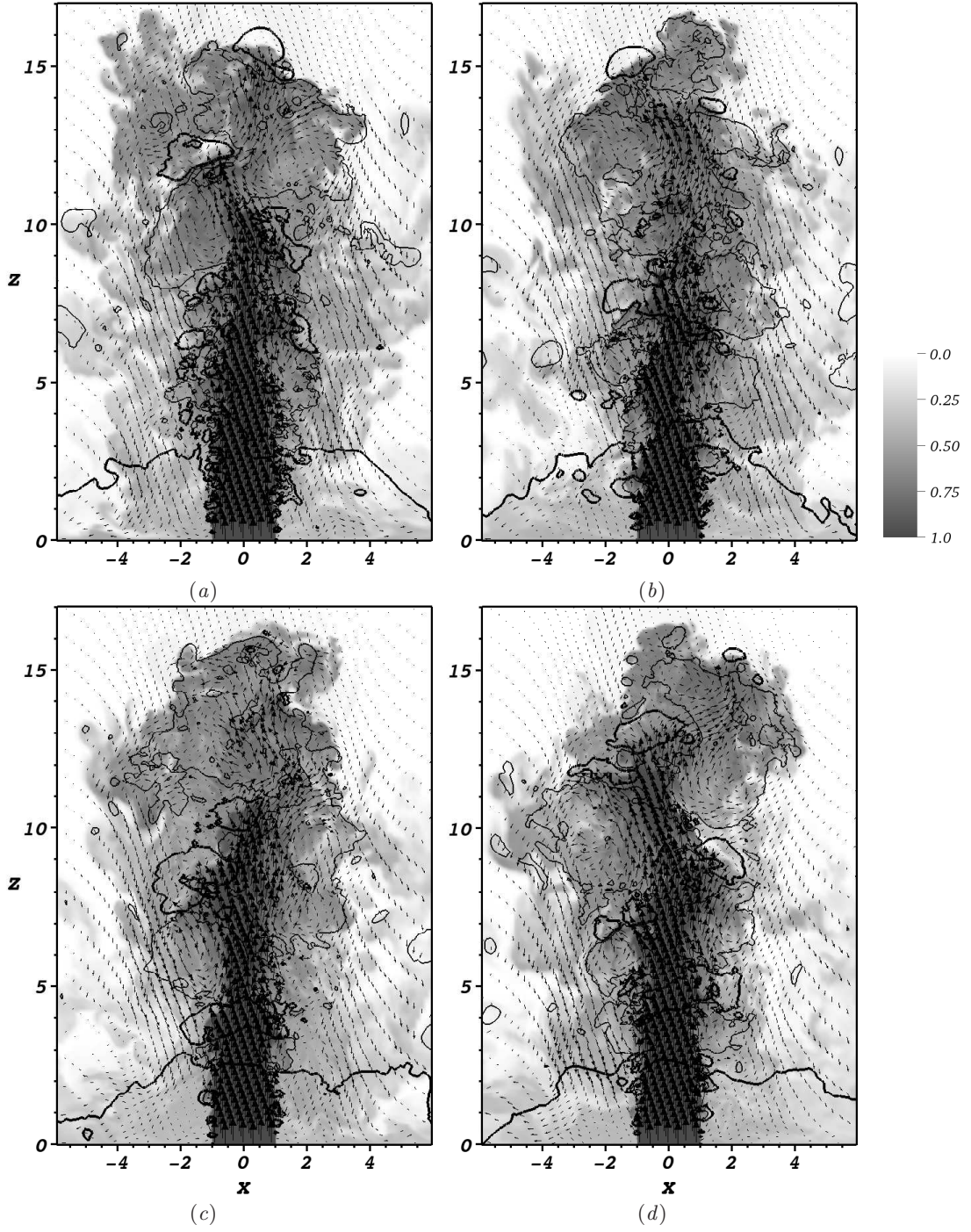
Figure 5: Flow structure of $Fr = 7.0$ simulation from $tU_0/R = 228$ (a) in increments of $tU_0/R = 14.7$ (a-d). Shading indicates ϕ with scale given above. Thicklines give $p/\rho U_0^2 = 0.015$ contors, thin lines give $p/\rho U_0^2 = -0.015$.
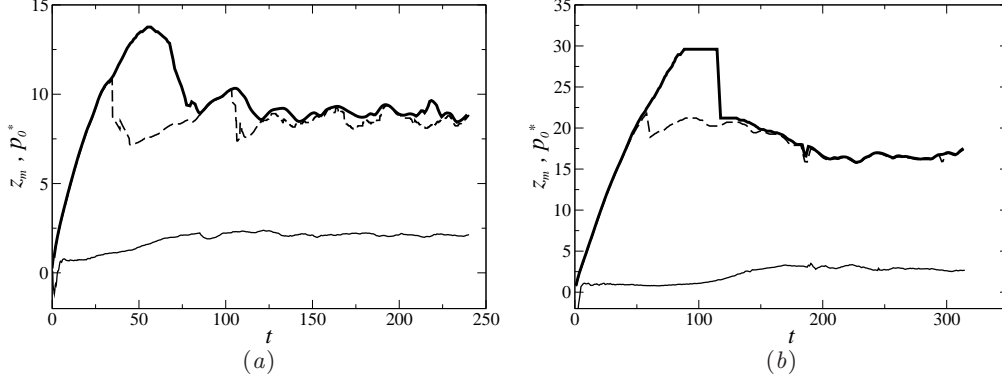
Figure 6: Time evolution of fountain height at $r = 0$ and normalised source pressure head $p_0^* = p_0 Fr^2$, at $r = 0$ and $z = 0$ for (a) $Fr = 4$ and (b) $Fr = 7$. $p_0^*(t)$ is indicated by thin-solid lines. $z_m(t)$ given by the maximum location of $\phi = 0.1$ and minimum location of $\phi = 0.1$, as indicated by thick solid line and dashed-line respectively. Scaling as indicated on axis.

potential core which extends to $z = 4$ where it meets the cap region while Kaye and Hunts work suggests that the weak–forced transition is at $Fr = 3$. This suggests that the fountain penetration height may follow the linear Froude number scaling before the flow is fully forced as would be defined by the physics of the mixing and entrainment in the structure.

5. Discussion

5.1. *Flow Statistics*

The results have been interpolated onto a cylindrical coordinate system (r, z, θ) and statistics calculated. The vertical profiles of the Reynolds stresses and mean flow quanitites are given in figure 8 along $r = 0$. In both $Fr = 4$ and $Fr = 7$, the temperature drops nearly lineraly from $z = 5$, before dropping rapidly at the end of the cap region. The centerline velocity appears to decrease with three behaviors. At $Fr = 7$ from $z \approx 0 - 9$ the velocity decreases slowly, from $z \approx 9 - 15$ the decrease is nearly linear and from $z \approx 15 - z_m$ the velocity drops quickly. This is discussed further in §6.

In $Fr = 4$, in figure 8(a), the shear layer does not fully develop before the cap region. The Reynolds stresses and $\overline{\phi' \phi'}^{0.5}$ peak first at $z = 6.8$ where the large eddy structrues from the down flow and cap region penetrate the inner flow stream advecting downflow fluid into the upflow. At $z = z_m$ intermitency in the location of the interface casues a spike in $\overline{\phi' \phi'}^{0.5}$.

In $Fr = 7$, in figure 8(b), $\overline{u_z u_z}^{0.5}$ peaks at $z = 10$ and then declines towards $z = z_m$. The sclar fluctuation $\overline{\phi' \phi'}^{0.5}$ and $\overline{u_r u_r}^{0.5}$ $\overline{u_t u_t}^{0.5}$ are nearly constant in magnatude between $z = 10 - z_m$, while . $\overline{u_z u_z}^{0.5}$ decreases more slowely than $\overline{u_z}$. At $z = z_m$, defined as the pont where where $\overline{u_z} = 0$, $\overline{\phi' \phi'}^{0.5}$ peaks with flow intermitency and the Reynolds stresses are non-zero until above $z \approx 20R$. The ratio of $\overline{u_z u_z}^{0.5}/\overline{u_z}$ increases with height and the flow becomes increasly.

The radial profiles of the the mean radial profiles of $\overline{u_z}$, $\overline{u_r}$ and $\overline{\phi}$ are given at different axial locations in figure 9(a-d)for $Fr = 4$ and in 10 for $Fr = 7$. The Reynolds stresses are
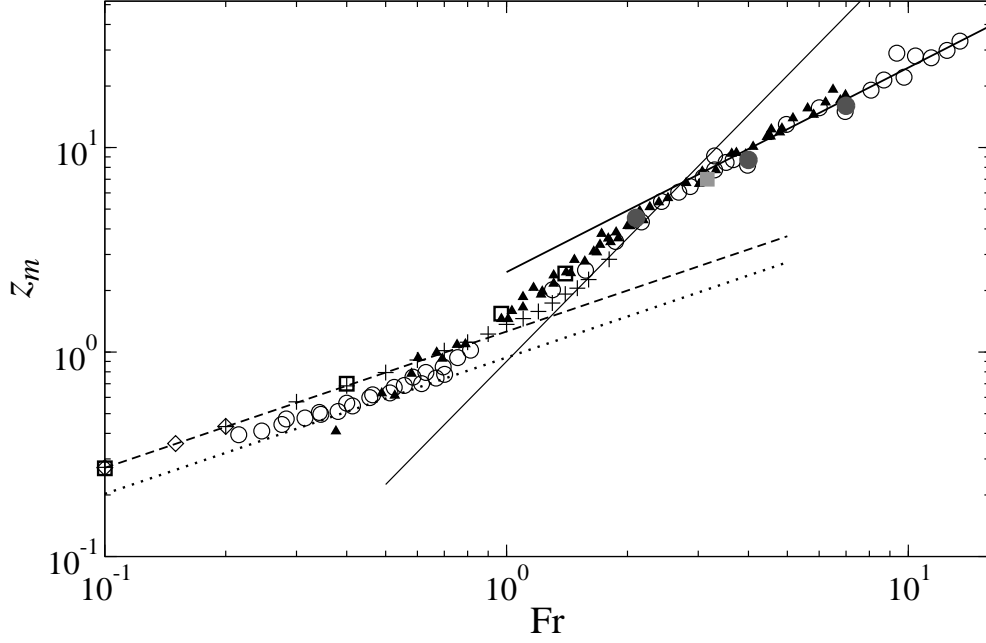
Figure 7: Normalised fountain penetration height with Froude number where the dashed-line is $1.26Fr^{2/3}$Lin & Armfield (2000b), the dotted-line $0.94Fr^{2/3}$Kaye & Hunt (2006), the thin-solid-line $0.9Fr^2$ Kaye & Hunt (2006) and the thick-solid-line $2.46Fr$ Turner (1966). Data symbols indicate,○Kaye & Hunt (2006),◇Lin & Armfield (2000b),+Lin & Armfield (2000a)(uniform source velocity profile),▲Zhang & Baddour (1998),■Cresswell & Szczepura (1993), □Williamson *et al.* (2010) and ● are present simulations
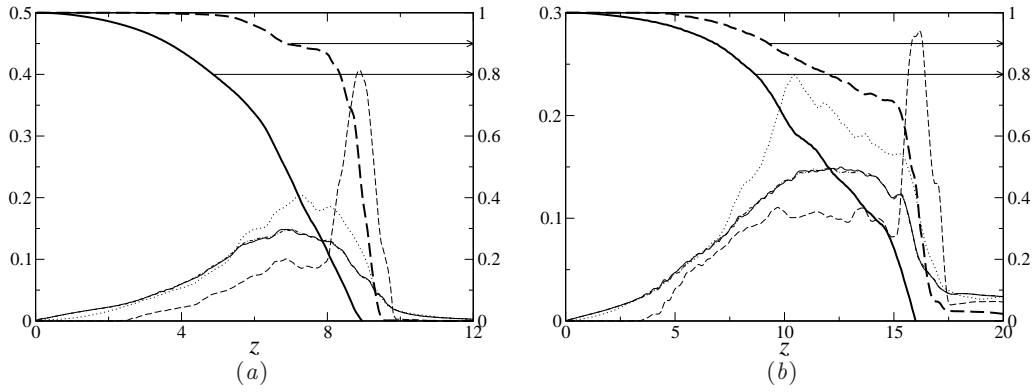

Figure 8: $\overline{u_z'u_z'}^{0.5}$-dotted line, $\overline{u_r'u_r'}^{0.5}$-thin solid line, $\overline{u_\theta'u_\theta'}^{0.5}$-dash dotted line, $\overline{\phi'\phi'}^{0.5}$-dashed line, $\overline{u_z}$-thick line ϕ-thick dashed line for $Fr = 4$ (a) and $Fr = 7$ (b).
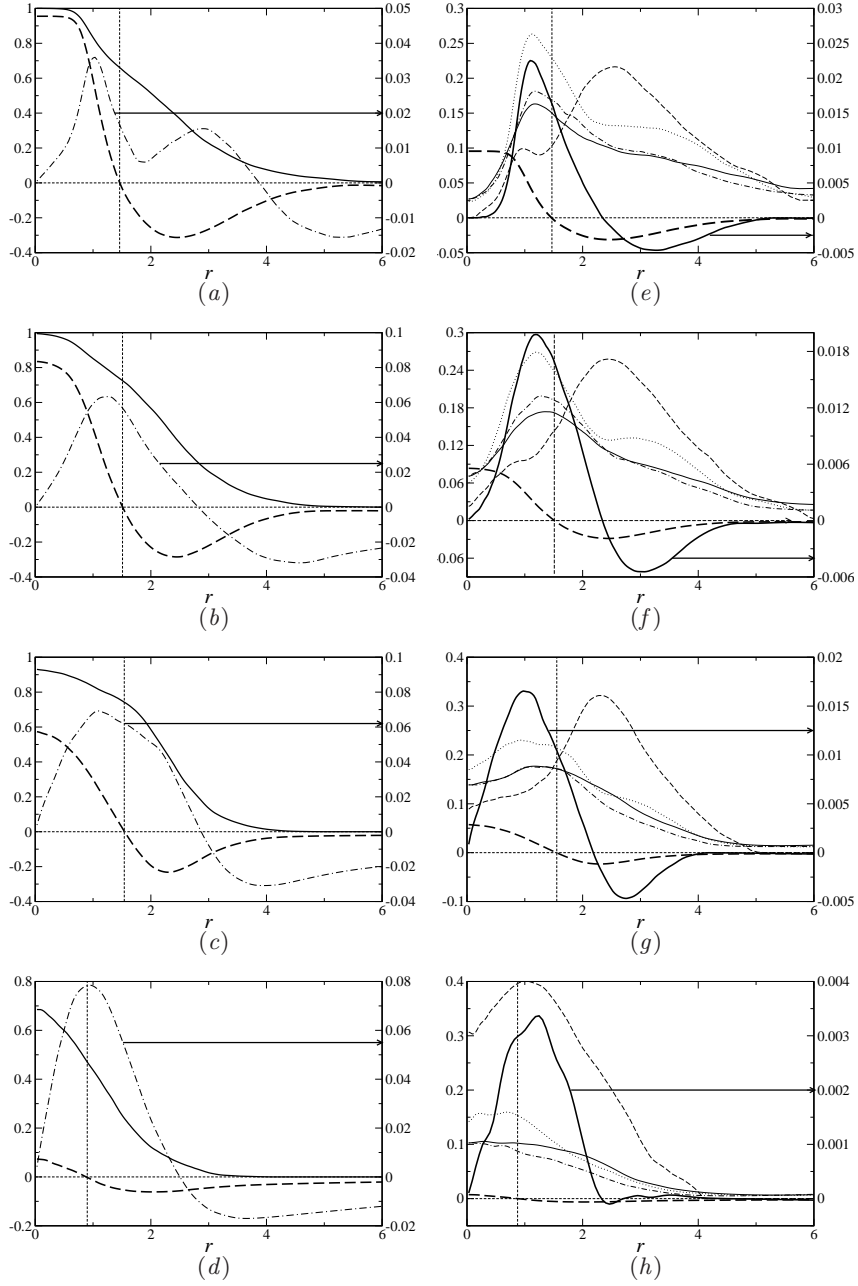
Figure 9: $Fr = 4$ radial profiles of: (a-d) u_z-thick dashed line, u_r-dash-dotted line, ϕ-solid line; (e-h) $\overline{u_z' u_z'}^{0.5}$-dotted line, $\overline{u_r' u_r'}^{0.5}$-thin solid line, $\overline{u_\theta' u_\theta'}^{0.5}$-dash-dotted line, $\overline{u_r' u_z'}^{0.5}$-thick line, $\overline{\phi' \phi'}^{0.5}$-dashed line, $\overline{u_z}$-thick dashed line. Plots are given at $z = 2.5$ (a,e), $z = 4.5$ (b,f), $z = 6.5$ (c,g), $z = 8.5$ (d,h). Straight thin dashed line indicates IF/OF boundry and x-axis.
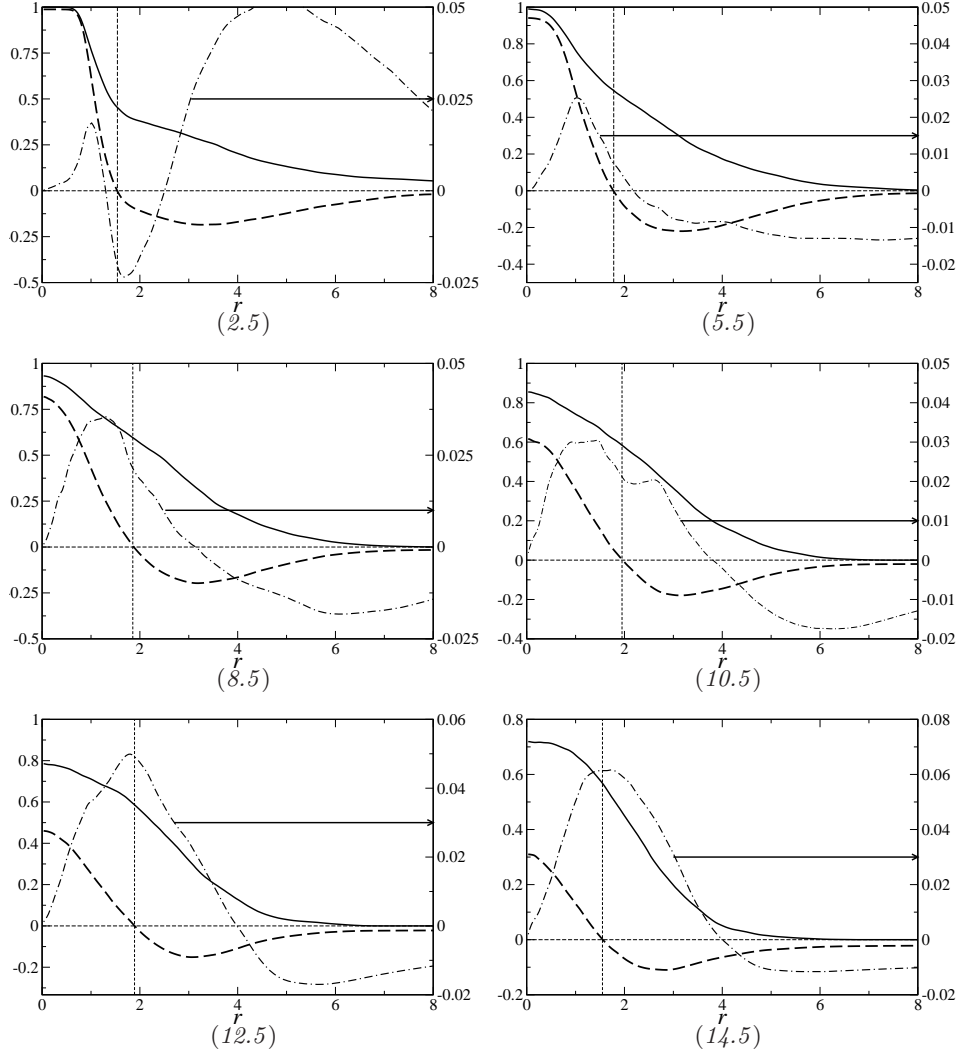
Figure 10: $Fr = 7$ radial profiles of $\overline{u_z}$-thick dashed line, $\overline{u_r}$-dash-dotted line, $\overline{\phi}$-solid line. Plots are given at $z = 2.5$ (a), $z = 5.5$ (b), $z = 8.5$ (c), $z = 10.5$ (d), $z = 12.5$ (e) and $z = 14.5$ (f).

given in figure 9(e-f) for $Fr = 4$ and in figure 11 for $Fr = 7$. The statistics are normalised by W_0. Other choices would be the local centerline velocity or the local mean difference betwen the upflow and downflow, but since the flow is not self-similar the inlet condition is a simpler quantity and allows direct comparison with Cresswell & Szczepura (1993) and Mizushina *et al.* (1982).

The flow development is similar to that in a free jet Boguslawski & Popiel (1979). $\overline{u_r u_r}^{0.5}$ is approximately equal to $\overline{u_\theta u_\theta}^{0.5}$ at most locations in both simulations. $\overline{u_z u_z}^{0.5}$ peaks at the center line at $z \approx 10.5$ where the shear layers merge. There is a double peak in the radial profile of $\overline{\phi'\phi'}^{0.5}$ before $z = 10.5$ for $Fr = 7$ and before $z = 4.5$ for $Fr = 4$. The inner most peak occurs in the developing IF while the secodn peak occurs in the OF. Above these locations there is only the single peak in the OF. There is no
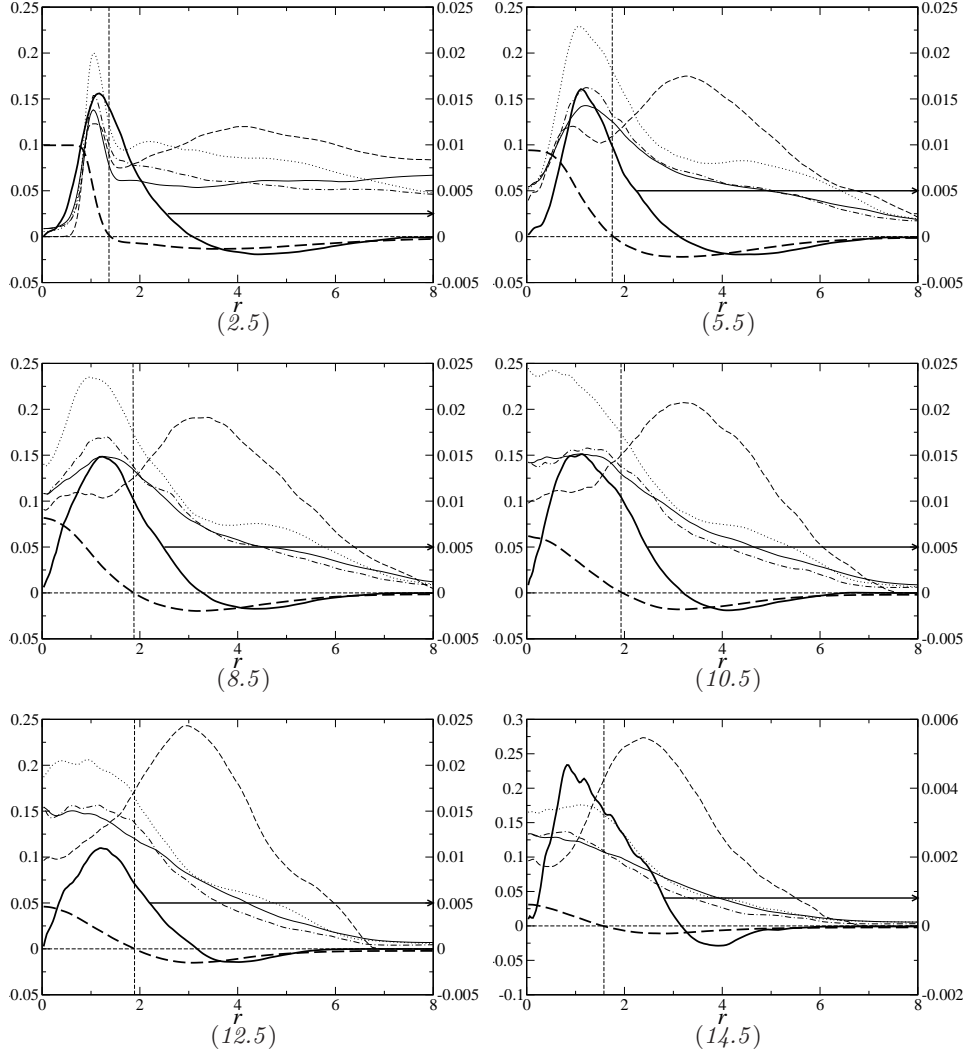
Figure 11: $Fr = 7$ radial profiles of $\overline{u'_z u'_z}^{0.5}$-dotted line, $\overline{u'_r u'_r}^{0.5}$-thin solid line, $\overline{u'_\theta u'_\theta}^{0.5}$-dash-dotted line, $\overline{u'_r u'_z}^{0.5}$-thick line, $\overline{\phi'\phi'}^{0.5}$-dashed line, $\overline{u_z}$-thick dashed line. Plots are at $z = 2.5$ (*a*), $z = 5.5$ (*b*), $z = 8.5$ (*c*), $z = 10.5$ (*d*), $z = 12.5$ (*e*) and $z = 14.5$ (*f*).

flow similarity in the IF or mixed region between the IF and OF with the flow developing along the trajectories of both flows. The possibility or partial flow similarity in the OF is examined in §6.

6. Entrainment

The fountain streams have been identified in figure 12 (*a*) and (*b*) for $Fr = 4$ and $Fr = 7$. The IF/OF boundry, r_{io} is defined as the radial location where $\overline{u_z} = 0$. The radial location r_d, where the maximum downward velocity in the OF occurs is indicated in figure 12. The best definition of the boundry between the OF/AF, r_{oa} is less clear. In an ideal pure plume $r u_r$ is a constant so it should not matter and the plume width B is
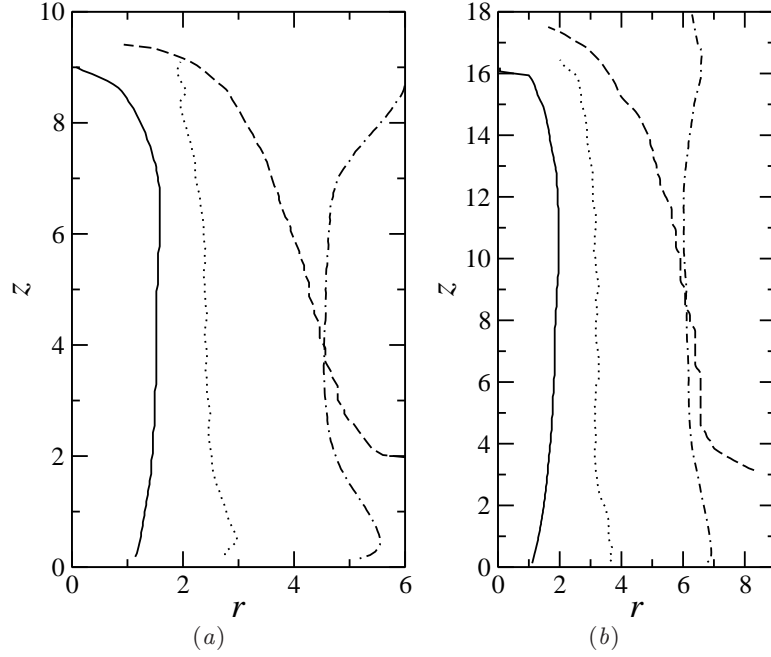
Figure 12: Boundries between flow streams in $Fr = 4$ (a) and $Fr = 7$ (b). Thin solid line-IF/OF boundry where $\overline{u_z} = 0$; dotted line indicates $r_d(z)$; dashed line-OF/AF boundry where $\overline{\phi} = 0.025$; dashed-dotted line indicates $B_{1/2} + r_d$.

usually obtained from $\sqrt{(b^2 W)^2/(b^2 W^2)}$. The equivalent length scale for a fountain OF halfwidth is,

$$B_{1/2} = \left(\left(2 \int_{r_d}^{r_{\text{lim}}} wrdr \right)^2 \Big/ \left(2 \int_{r_d}^{r_{\text{lim}}} w^2 rdr \right) + r_d^2 \right)^{1/2} - r_d, \tag{6.1}$$

where

$$b^2 W = 2 \int_{r_{io}}^{r_{oa}} wrdr, \tag{6.2}$$

$$b^2 W^2 = 2 \int_{r_{io}}^{r_{oa}} w^2 rdr. \tag{6.3}$$

The simulated domain is finite so the integrals in (6.1) are evaluated to the edge of the domain $r = r_{\text{lim}}$. The total distance from the centerline is $r_{oa} = B_{1/2} + r_d$. This definition of r_{oa} is plotted in figure 12. A second definitaion defined as the location where $\phi = 0.025$ is also given in figure 12. The comparison between this definitaion and that based on (6.1) is only close over a small portion of the OF height with large deviations at the top and bottom of the flow height. This may be because of the influence of intrusion outflow is to create additional circulation so entrainment is not the same as that of free shear plume. In both the $Fr = 4$ and 7 results the inner upflow stream is of nearly constant width. It expands rapidly over the $z = 0 - 2$ and then expands very slowly at approximately $dr/dz \approx 0.04$. The maximum velocity in the OF is located at $r \approx 2.5$ and $r \approx 3.0$ independent of z for $Fr = 4$ and $Fr = 7$ respectively. The IF contracts after $z = 6$ and
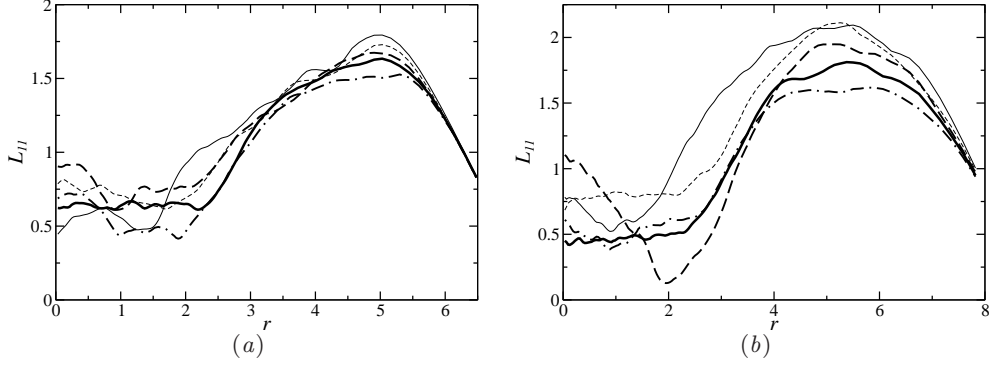
Figure 13: $L11$ (6.4) for $Fr = 4$ (a) and $Fr = 7$ (b). The lines dash-dotted, thick-solid, thick-dashed, thin-dashed, thin-solid indicate $z = 3$, $z = 4$, $z = 5$, $z = 6$, $z = 7$ in (a) $z = 4$, $z = 6$, $z = 8$, $z = 10$, $z = 12$ in (b).

$z = 10$ for $Fr = 4$ and $Fr = 7$ respectively. The downflow expands at the base of the fountain as the plume moves into the intrusion.

It is attractive from a modelling point of veiw to treat the OF as an indipendent plume. The integral length scale L_{11} for radial varience $\overline{u'_r(r,z)u'_r(r+dr,z)}$ is given as,

$$L_{11}(r,z) = \int_r^{r_{\lim}} R_{11}(r,z,dr)dr, \qquad (6.4)$$

where

$$R_{11}(r,z,dr) = \frac{\overline{u'_r(r,z)u'_r(r+dr,z)}}{\sqrt{u'_r(r,z)}\sqrt{u'_r(r+dr,z)}}. \qquad (6.5)$$

This result is plotted in figure 13 (a) and (b) for $Fr = 4$ and $Fr = 7$ respectively. The length scale is relatively flat across the IF region but rises sharply at $r = r_{io} - r_d$. In the OF plume like area over $r = 3 - 8$ the length scale increases to $L_{11} = 2$ for $Fr = 7$ and $L_{11} = 1.5$ for $Fr = 4$, approximately half the width of the OF stream. This suggests the connection between the structures in the IF and the OF is fairly indirect. In figure 14 some bulk statistics at $Fr = 7$ are normalised by local flow variable values at $r = r_d$ and the length scale $B_{1/2} + r_d$. From $z = 5 - 11$ the curves collapse relatively well suggesting at least partical flow similarity. Other quantities such as $\overline{u'_r u'_r}$ and $\overline{u_r}$ compare very poorly.

The mean entrainment $\overline{\alpha}$ between the streams is calculated as,

$$\alpha = -s\overline{u_r}/W. \qquad (6.6)$$

where $\overline{u_r}$ is obtained at r_{io} for IF/OF entrainment and r_{oa} for OF/AF entrainment. The entrainment direction is into the OF from both the AF and the IF over most of the height. This direction is taken as positive so $s = -1$ for the AF/OF boundry and $s = 1$ for the IF/OF boundry. The bulk OF stream velocity is given as,

$$W = \frac{b^2 W^2}{b^2 W}. \qquad (6.7)$$

The entrainment rate is plotted in figure 15 (a-b) for $Fr = 4$ and $Fr = 7$ respectively. Results for multiple definitions of r_{oa} are presented and the sensitivity of the entrainment rate to boundry location is also given. The entrainment profile from the AF with $r_{oa} =$
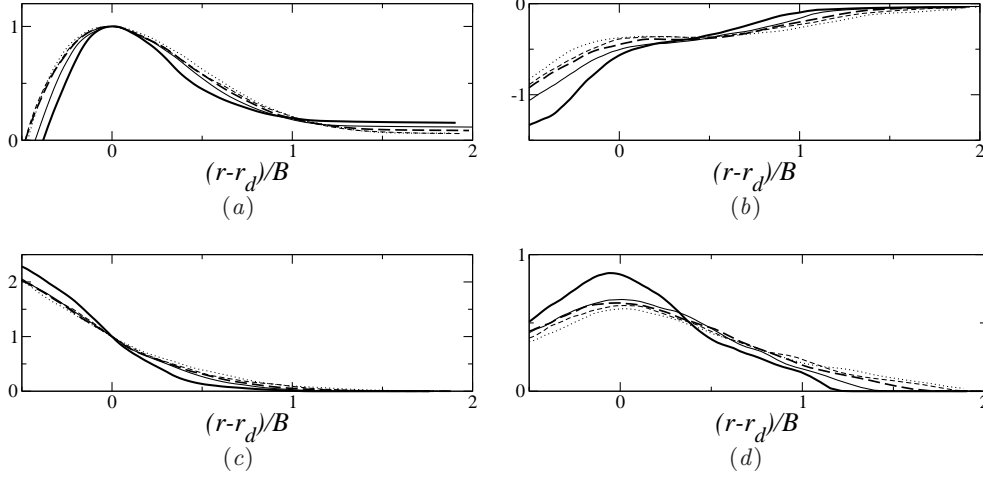
Figure 14: Similarity of flow statistics in the OF at $Fr = 7$. (a) $U_z(r,z)/U_z(r_d,z)$, (b) $\overline{u'_z(r,z)u'_z(r,z)}^{0.5}/U_z(r_d,z)$, (c) $\phi(r,z)/\phi(r_d,z)$, (d) $\overline{\phi'(r,z)\phi'(r,z)}^{0.5}/\phi(r_d,z)$. Dotted line $z = 5$, thin dashed line $z = 7$, thick dashed line $z = 9$, thin solid line $z = 11$, thick solid line $z = 13$.

r_{lim} is also shown in figure 15. The entrainment rate is not sensitive to the location of the boundary.

The entrainment profiles illustrate distinct regions of behavior. The base outflow up to $z = 2$ and $z = 4$ for $Fr = 4$ and $Fr = 7$ respectively, where there is entrainment into the IF from the OF and from the OF into the base intrusion or AF. Above this up to $z \approx 8$ and $z \approx 14$ for $Fr = 4$ and $Fr = 7$ respectively entrainment from the AF to the OF approaches the nearly constant value of $\overline{\alpha} = 0.1 - 0.2$. Over this region there is low but increasing entrainment into the OF from the IF. Above region to the top of the fountain, the entrainment regime in both streams is dominated by ejection of fluid from the cap region, so the OF receives fluid from the IF and the AF receives fluid from the OF. The nearly constant entrainment into the OF from the AF supports the iea that the dynamic of this stream is similar to a plume. The behavior near the intrusion and in the cap region varies but here entrainment has a different behavior and (6.6) does not have any meaning. The plume is not symmetric about the maximum downflow velocity line. The outer flow expands freely while the inner region is confined by the upflow.

List (1982) give entrainment into a plane bouyant plume with $\alpha = 0.14$. Entrainment into a axisymemtric plume is $\alpha = 0.11$. The higher entrainment coefficient found here may be due to the ambient circulation or the more unsteady pulsing behavior of the ejection into the downflow. The dense fluid enters the downflow with higher radial velocity and therfore once it accelerates down is able to draw more ambient fluid in behind each pulse. This process is illustrated in movie 3 (available with the online version of the paper).

The vertical flux of velocity, momentum and buoyancy for the IF and OF flow streams, given by

$$Q = 2 \int_{r_1}^{r_2} wr\,dr \tag{6.8}$$

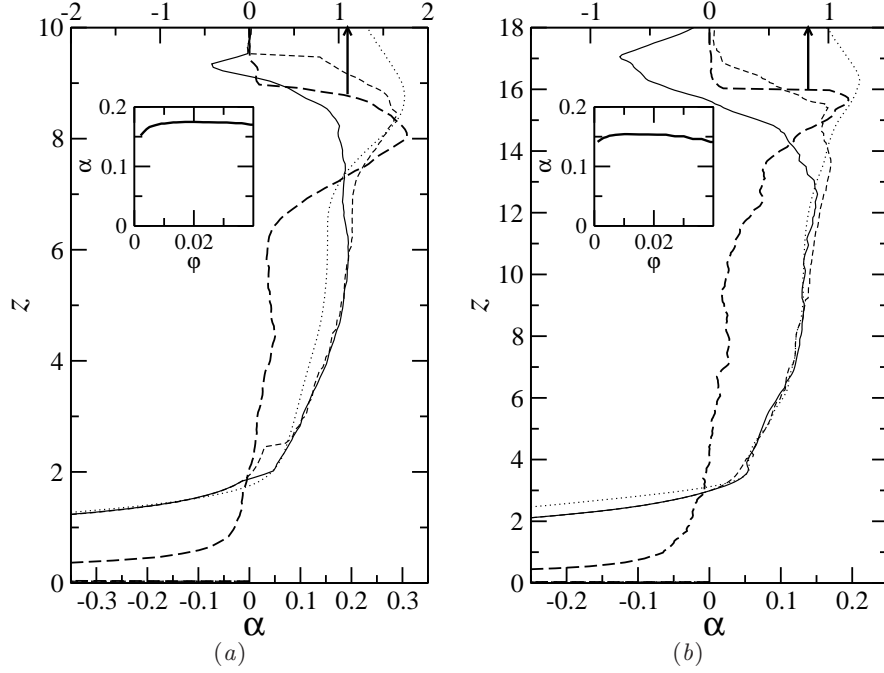$$M = 2 \int_{r_1}^{r_2} w^2 r\,dr \tag{6.9}$$

Figure 15: Mean entrainment rates for $Fr = 4$ (a) and $Fr = 7$ (b). Thick dashed line is entrainment into OF from IF. Solid line, thin dashed line and dotted line indicate entrainment into OF from the AF with the OF/AF boundry r_{oa} defined by the location of $\phi = 0.025$, $\phi = 0.005$ and $r_{\lim}$ respectively. Inner plot indicates sensitivity of AF entrainment to r_{oa}, as defined by ϕ, at $z = 5$ and $z = 11$ for $Fr = 4$ (a) and $Fr = 7$ (b) respectively.

$$F = 2 \int_{r_1}^{r_2} w\phi r dr, \qquad (6.10)$$

are plotted in figure 16, where $r_1 = 0$ and $r_2 = r_{io}$ for the IF stream and $r_1 = r_{io}$ and $r_2 = r_{\lim}$ for the OF stream. At $Fr = 7$ in the IF the flux of buoyancy increases over $z = 0$-3 and mass flux increases over $z = 0$-4 with entrainment from the OF. From $z = 5$-12 the IF expands weakly with weak detrainment into the OF. Above $z = 12$, the IF Q decreases rapidly with radial flow into the OF. The transport of momentum is examined in §6.1.

6.1. *Momentum Balance*

The vertical momentum equation is,

$$\underbrace{\left(\overline{u_r}\frac{\partial \overline{u_z}}{\partial r} + \overline{u_z}\frac{\partial \overline{u_z}}{\partial z} \right)Fr^2}_{A} \quad + \quad \underbrace{\frac{\partial \overline{p}}{\partial z}Fr^2}_{P} \quad \underbrace{-\frac{1}{Re}\left(\frac{1}{r}\frac{\partial}{\partial r}\left(r\frac{\partial \overline{u_z}}{\partial r} \right) + \frac{\partial^2 \overline{u_z}}{\partial z^2} \right)Fr^2}_{V}$$

$$+ \quad \underbrace{\left(\frac{1}{r}\frac{\partial r\overline{u_z'u_r'}}{\partial r} + \frac{\partial \overline{u_z'u_z'}}{\partial z} \right)Fr^2}_{D} \quad + \quad \underbrace{\overline{\phi}}_{B} = 0. \quad (6.11)$$
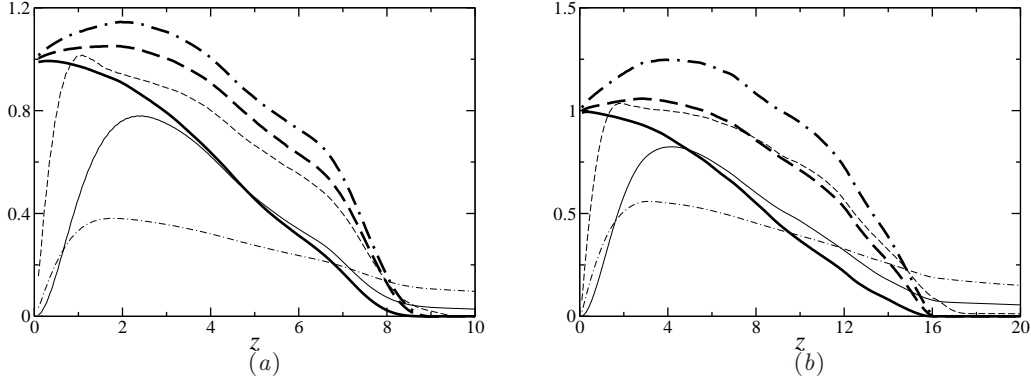
Figure 16: Q-dashed-dotted line, M-solid line, F-dashed line for IF stream (thick lines) and OF stream (thin lines) at $Fr = 4$ (a) and $Fr = 7$ (b).

The balance terms from (6.11) are given in figure 17 (a) for $Fr = 4.0$ and figure 17 (b) for $Fr = 7$. The terms are filtered with a discrete top hat filter of width $\overline{G} = 3\Delta X/R_0$, to remove grid scale oscillations remaining in the statistics which effect the clarity of the plots. In figure 18 the integrated balance terms are given for the IF and OF.

In figure 17, from $z = 1 - 3$ the balance terms have the same charactersitics as the weak fountains results presented in Williamson *et al.* (2010) for $Fr = 0.4 - 2.1$. At the source at $z = 0$ and $r = 0$, the axial momentum balance is $\partial \overline{p}/\partial z \approx \phi/Fr^2$. This axial pressure gradient is mainly due to the presence of the intrusion flow and is very small in the initial flow development before the OF is formed. For $Fr = 7$ from $z = 0 - 5$ at $r = 0$, the adevctive term increases nearly linearly at the expense of the pressure gradient until at $z = 5$ the balance is approaximately $\overline{u_z}\partial \overline{u_z}/\partial z = \phi/Fr^2$. In the mixing region, $\overline{u_r}\partial \overline{u_z}/\partial r$ is the more important term. The turbulent diffusion term increases rapidly at $z = 5$ and peaks at $z = 6 - 7$ where $\overline{u_z' u_z'}$ reaches its maximum value. Here $P \approx 0$ so $D + B \approx u_z \partial u_z/\partial z$ from $r = 0 - 1$. For $Fr = 4.0$, the diffusion term is slightly smaller in magnitude to the bouancy term while for $Fr = 7.0$ the diffusion term is more significant.

For $Fr = 7.0$, there is a seperate behavior between the merging of the shear layer at $z = 10$ and the cap region. In figure 18 at $z = 10.5$, the term $\int_{R_1}^{R_2} 2Fr^2\partial(r\overline{u_z' u_z'})/\partial r \, dr$ becomes negative. $\int_{R_1}^{R_2} 2Fr^2\partial(r\overline{u_z' u_r'})/\partial r \, dr = r_{io}\overline{u_z' u_r'}_{rr}$ is positive. The axial gradient of the axial Reynolds stress $\partial\overline{u_z' u_z'}/\partial z$, is significant unlike in non-buoyant jet flow where it is typically neglected in the integral models (e.g. Morton 1959).

A different type of behavior at the top of the fountain where the fluid is forced radaily into the downflow. Here, in both $Fr = 4$ and $Fr = 7$, diffusion term changes sign. $\partial\overline{u'v'}/\partial r + \overline{u_z' u_r'}/r \rightarrow 0$ and $\partial\overline{u_z' u_z'}/\partial z$ becomes more negative and overall the diffusion term becomes negative. This small region is very unsteady. The pressure gradient becomes positive here. For $Fr = 7$, the top of the fountain is a complex balance bewteen all the terms. Bouyancy and pressure oppose the diffusion of momentum from the core. At the top of the fountain the pressure rises and the flow stagnates.

Vertical momentum transported into the downflow via $\partial\overline{u_z' u_r'}/\partial r$. The results in a balance of $\partial\overline{u_z' u_r'}/\partial r \approx \phi/Fr^2$. Near the source the axial pressure gradient balances the buoyancy term where the intrusion forms.

In this way the forced regime appears to be comprised of the three regions, the first being the entrance region where pressure and advection dominate. The second where teh
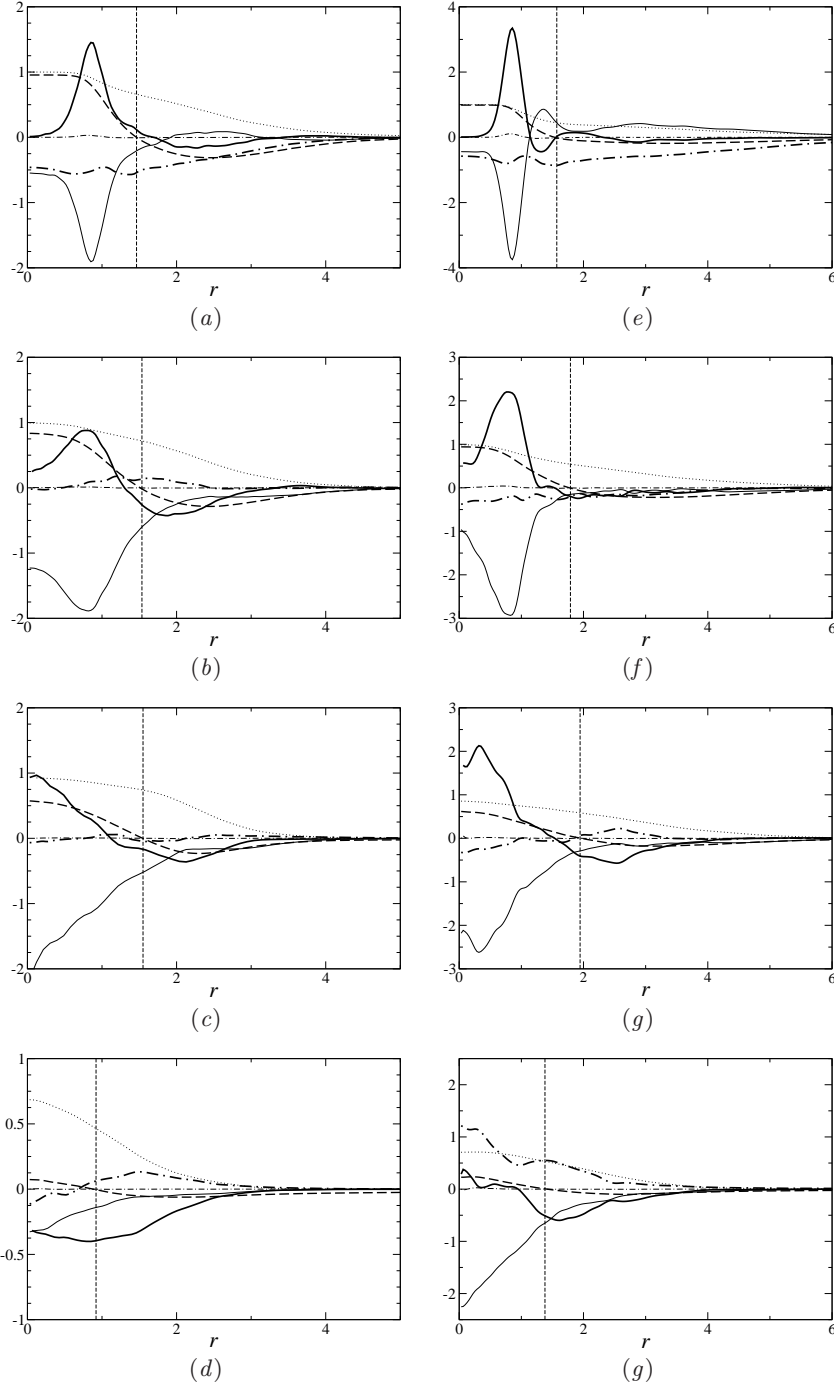
Figure 17: Vertical momentum balance terms for $Fr = 4$ (a-d) $Fr = 7$ (e-h). Plots are at $z = 2.5, 4.5, 6.5, 8.5$ (a-d) and $z = 2.5, 5.5, 10.5, 15$ (e-h). Solid line: A, thick solid line: D, dotted line: B, thick dashed dotted line: P, thin dashed dotted line: V. Thick dashed line: $\overline{u_z}$ and thin dashed vertical line indicates r_{io}.
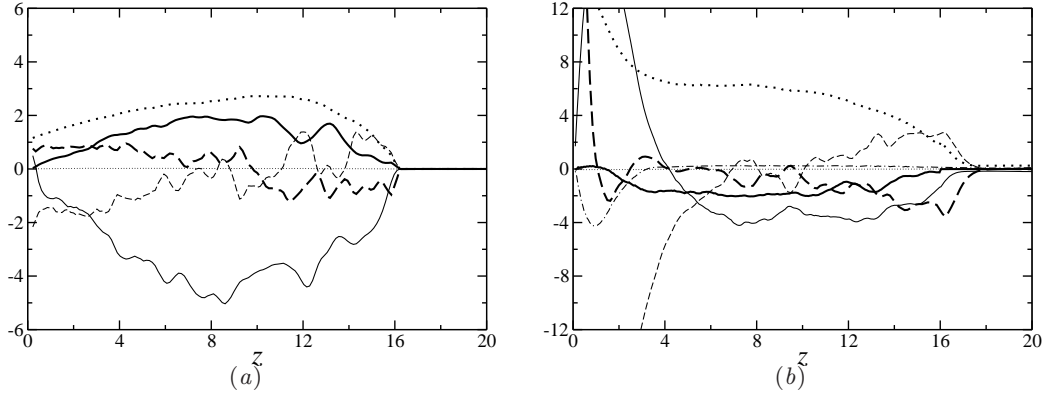
Figure 18: Vertical momentum balance for of the IF (a) and OF (b) at $Fr = 7$. Thick solid line: $\int_{R_1}^{R_2} 2Fr^2 \partial(r\overline{u'_z u'_r})/\partial r \, dr$, thick dashed line: $\int_{R_1}^{R_2} 2Fr^2 \partial(r\overline{u'_z u'_z})/\partial z \, dr$, thin dashed line: $\int_{R_1}^{R_2} 2Fr^2 \partial(rP)/\partial z \, dr$, thin dotted line: $\int_{R_1}^{R_2} 2V dr$ and thin solid line: $\int_{R_1}^{R_2} 2Fr^2 \partial(r\overline{u_z}^2)/\partial z \, dr$, thin dash-dotted: $\int_{R_1}^{R_2} 2Fr^2 \partial(r\overline{u_z}\,\overline{u_r})/\partial r \, dr$ and thick dotted line: $\int_{R_1}^{R_2} 2(r\overline{\phi})dr$.
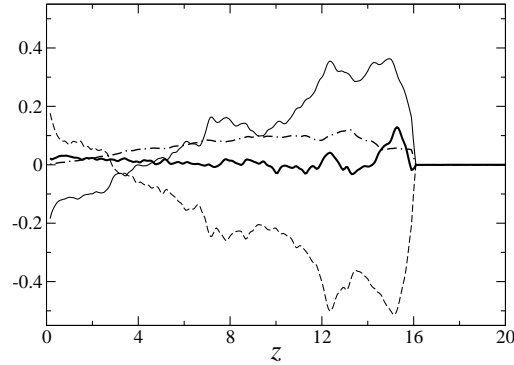

Figure 19: Axial scalar transport equation for of the IF at $Fr = 7$.

potential core ends and diffusion of momentum and buoynacy decelerate the flow. The thrid region is a cap region where diffusion works against byuoancy but the axial pressure gadient regmains low.

Previous modelling attempts, Abraham (1967), Bloomfield & Kerr (1998, 2000),Lin & Linden (2005)

7. Conclusions

At Fr=4.0-7.0 the shear layer meger at $z/r = 5$ and diffusio is important through the fountain height. The cap region is diffusion/nuoynacy balance as is the downflow stream.

A quantitative description of the behavior difference from jet or plume flow. interaction of the flow streams.

This work has demonstrated that the flow iacross $Fr = 4-7$ is still developing. Further

results at higher Froude numebrs are needed do understand the how the intereactions in the flow change once the flow is in the forced regime throughout most of its height.

REFERENCES

ABRAHAM, G. 1967 Jets with negative buoyancy in homogeneous fluid. *J. Hyd. Res.* **5**, 235–248.

BADDOUR, R. E. & ZHANG, H. 2009 Density effect on round turbulent hypersaline fountain. *J. Hydraul. Eng.* **135**, 57–59.

BAINES, W. D., TURNER, J. S. & CAMPBELL, I. H. 1990 Turbulent fountains in an open chamber. *J. Fluid Mech.* **212**, 557–592.

BLOOMFIELD, L. J. & KERR, R. C. 1998 Turbulent fountains in a stratified fluid. *J. Fluid Mech.* **358**, 335–356.

BLOOMFIELD, L. J. & KERR, R. C. 2000 A theoretical model of a turbulent fountain. *J. Fluid Mech.* **424**, 197–216.

BOGUSLAWSKI, L. & POPIEL, CZ. O. 1979 Flow structure of the free round turbulent jet in the initial region. *J. Fluid Mech.* **90**, 531–539.

CAMPBELL, I. H. & TURNER, J. S. 1989 Fountains in magma chambers. *J. Petrol.* **30**, 885–923.

CRESSWELL, R. W. & SZCZEPURA, R. T. 1993 Experimental investigation into a turbulent jet with negative buoyancy. *Phys. Fluids A* **5**, 2865–2878.

DEMETRIOU, J. D. 1978 Turbulent diffusion of vertical water jets with negative buoyancy (in greek). PhD thesis, National Technical University of Athens, Department of Civil Engineering.

KAMINSKI, E., TAIT, S. & CARAZZO, G. 2005 Turbulent entrainment in jets with arbitrary buoyancy. *J. Fluid Mech.* **526**, 361–376.

KAYE, N. B. & HUNT, G. R. 2006 Weak fountains. *J. Fluid Mech.* **558**, 319–328.

LEONARD, B. P. & MOKHTARI, S. 1990 Beyond first-order upwinding: the ultra-sharp alternative for non-oscillatory steady state simulation of convection. *Int. J. Numer. Meth. Engng* **30**, 729–766.

LIN, W. & ARMFIELD, S. W. 2000a Direct simulation of weak axisymmetric fountains in a homogeneous fluid. *J. Fluid Mech.* **403**, 67–88.

LIN, W. & ARMFIELD, S. W. 2000b Very weak axisymmetric fountains in a homogeneous fluid. *Numer. Heat Transfer A* **38**, 377–396.

LIN, Y. J. P. & LINDEN, P. F. 2005 The entrainment due to a turbulent fountain at a density interface. *J. Fluid Mech.* **542**, 25–52.

LIST, E. J. 1982 Turbulent jets and plumes. *Ann. Rev. Fluid Mech.* **14**, 189–212.

MARUGÁN-CRUZ, C., RODRÍGUEZ-RODRÍGUEZ, J. & MARTÍNEZ-BAZÁN, C. 2009 Negatively buoyant starting jets. *Phys. Fluids* **21**, 117101.

MIZUSHINA, T., OGINO, F., TAKEUCHI, H. & IKAWA, H. 1982 An experimental study of vertical turbulent jet with negative buoyancy. *Wärme-und Stoffübertragung* **16**, 15–21.

MORTON, B. R. 1959 Forced plumes. *J. Fluid Mech.* **5**, 151–163.

PANTZLAFF, L. & LUEPTOW, R. M. 1999 Transient positively and negatively buoyant turbulent round jets. *Exp. Fluids* **27**, 117–125.

SENDAN, R. A., BEHNIA, M. M. & ABREU, K. E. 1978 Temperatures in a heated air jet discharged downward. *Intl. J. Heat Mass Transfer* **21**, 1453–1458.

SUZUKI, Y. J., KOYAGUCHI, T., OQAWA, M. & HACHISU, I. 2005 A numerical study of turbulent mixing in eruption clouds using a three-dimensional fluid dynamics model. *J. Geophys. Res.* **110**.

TURNER, J. S. 1966 Jets and plumes with negative or reversing buoyancy. *J. Fluid Mech.* **26**, 779–792.

WILLIAMSON, N., ARMFIELD, S. W. & LIN, W. 2008a Direct numerical simulation of turbulent intermediate froude number fountain flow. *ANZIAM J.* **50**, C16–C30.

WILLIAMSON, N., ARMFIELD, S. W. & LIN, WENXIAN 2010 Transition behaviour of weak turbulent fountains. *J. Fluid Mech.* **xxx**, xxx.

WILLIAMSON, N., SRINARAYANA, N., ARMFIELD, S. W., MCBAIN, G. D. & LIN, W. 2008*b* Low-reynolds-number fountain behaviour. *J. Fluid Mech.* **608**, 297–317.

ZHANG, H. & BADDOUR, R. E. 1997 Maximum vertical penetration of plane turbulent negatively buoyant jets. *J. Eng. Mech.* **123**, 973–977.

ZHANG, H. & BADDOUR, R. E. 1998 Maximum penetration of vertical round dense jets at small and large Froude numbers. *J. Hydraulic Eng.* **124**, 550–553.